Parity-Forbidden Excitations of $Sr_2CuO_2Cl_2$ Revealed by Optical Third-Harmonic Spectroscopy

A. B. Schumacher,* J. S. Dodge,† M. A. Carnahan, R. A. Kaindl, and D. S. Chemla
Department of Physics, University of California at Berkeley, Berkeley, California 94720
and Materials Sciences Division, E. O. Lawrence Berkeley National Laboratory, Berkeley, California 94720

L. L. Miller
Ames Laboratory and Department of Physics, Iowa State University, Ames, Iowa 50011
(Received 9 March 2001; published 31 August 2001)

We present the first study of nonlinear optical third-harmonic generation (THG) in the strongly correlated charge-transfer insulator $Sr_2CuO_2Cl_2$. For fundamental excitation in the near infrared, the THG spectrum reveals a strongly resonant response for photon energies near 0.7 eV. Polarization analysis reveals this novel resonance to be only partially accounted for by three-photon excitation to the optical charge-transfer exciton, and indicates that an even-parity state at 2 eV, with a_{1g} symmetry, participates in the third-harmonic susceptibility.

DOI: 10.1103/PhysRevLett.87.127006 PACS numbers: 74.72.–h, 42.65.An, 42.65.Ky, 71.70.Ch

In a Mott insulator, antiferromagnetic interactions can make two particles more mobile than one, creating a strong pairing force that is the likely cause of high-T_C superconductivity. This basic insight has guided research on the high-T_C problem since its introduction by Anderson [1]. It also implies that optical excitations in Mott insulators must be treated differently from their band counterparts, as the same interactions that bind Cooper pairs in the metal will contribute to the binding of particle-hole pairs in the insulator. Inelastic x-ray scattering on $Ca_2CuO_2Cl_2$ lends support to this proposition, by showing that the bandwidth of particle-hole excitations is several times larger than that of the individual particle bandwidth [2]. Charge-transfer (CT) insulators possess additional, charge degrees of freedom, also discussed as a potential mechanism for high-T_C superconductivity [3,4].

While the most obvious optical feature in the insulating cuprates is the CT gap excitation near 2 eV, optically forbidden CT states should also exist, with a_{1g} (s) or b_{1g} ($d_{x^2-y^2}$) symmetry in $4/mmm$ [5–7]. These even-parity modes have been implicated in the anomalously large nonlinear optical coefficients observed in one-dimensional Mott and charge-transfer insulators, and in the nonlinear optical spectrum of La_2CuO_4 [8–10]. Parity-forbidden excitations with ligand field, or dd character, are also expected; these are intra-atomic excitations that result directly from strong correlations, in which the hole in the ground state (g) Cu($3d_{x^2-y^2}$) orbital is transferred to another Cu orbital of different symmetry. Even-parity excitations have been studied in the optical and Raman spectra of insulating cuprates, but the details of their line shapes, temperature dependence, and even their assignment has been controversial [11–13].

In this Letter, we employ nonlinear optical spectroscopy to determine the symmetry and spectrum of both even- and odd-parity states near the charge-transfer gap of $Sr_2CuO_2Cl_2$, a model insulating cuprate. Like the Raman tensor, the third harmonic generation (THG) tensor studied here is fourth rank, and contains symmetry information that is inaccessible to linear optics. Polarization analysis of the nonlinear optical response provides evidence for an even-parity state at approximately 2 eV, with a_{1g} symmetry, and allows us to estimate the magnitude of the dipole matrix element that couples this excitation to the CT exciton. The technique that we describe here is generally applicable to correlated insulators, and should provide valuable input into models of their electronic structure.

In our experiment, we completely characterize the THG tensor elements, $\chi^{(3)}(-3\omega;\omega,\omega,\omega)$, for the Cu-O plane of $Sr_2CuO_2Cl_2$. In this case, the nonlinear susceptibility tensor has two independent elements, $\chi^{(3)}_{xxxx}$ and $\chi^{(3)}_{xxyy}$, in general complex, for a driving optical field $\mathbf{E}(\omega)$ polarized in the plane. Throughout, we take x and y to correspond to coordinates aligned with the crystalline axes of $Sr_2CuO_2Cl_2$, with the z axis normal to the crystal and in the direction of propagation. The nonlinear polarization is given by

$$\begin{aligned} P_x(3\omega) &= \chi^{(3)}_{xxxx}E_x^3 + 3\chi^{(3)}_{xxyy}E_xE_y^2, \\ P_y(3\omega) &= \chi^{(3)}_{xxxx}E_y^3 + 3\chi^{(3)}_{xxyy}E_x^2E_y. \end{aligned} \tag{1}$$

It is useful to write the two tensor elements in terms of an amplitude and a phase: $\chi^{(3)}_{xxxx} = \kappa_{xx}e^{i\alpha}$, and $\chi^{(3)}_{xxyy} = \kappa_{xy}e^{i\beta}$, with the phase difference defined as $\delta = \beta - \alpha$.

We first measured the magnitude of the third harmonic susceptibility $|\chi^{(3)}_{xxxx}|$ at room temperature, as a function of fundamental photon energy. These and all other measurements described here were performed with a 250 kHz Ti:sapphire laser amplifier driving an optical parametric amplifier. To account properly for variations in pulse duration and mode profile as the laser wavelength is tuned, we compared the third harmonic intensity $I(3\omega)$ generated in $Sr_2CuO_2Cl_2$ with a quartz reference. We accounted for the $Sr_2CuO_2Cl_2$ absorption at 3ω in the limit $\ell \ll \lambda$,

$\Delta k\ell \approx 0$, appropriate here [14]. High-quality single crystals of $Sr_2CuO_2Cl_2$ [15] were cleaved to a thickness of $\ell \sim 100$ nm, and oriented crystallographically with x-ray diffraction. The quartz reference was a thin, $\ell = 150\ \mu$m, c-axis plate, whose absolute nonlinear susceptibility, $\chi^{(3)}_{xxxx}(\text{quartz}) = 3 \times 10^{-14}$ esu, is known independently [16]. The measured relative intensities, along with the resulting $|\chi^{(3)}_{xxxx}|$ of $Sr_2CuO_2Cl_2$ are shown in Fig. 1. The spectrum exhibits a broad $\approx$0.5 eV wide resonance at 0.7 eV, varying by more than a factor of 20 over the explored frequency range. Since the susceptibility $\chi^{(3)}(-3\omega;\omega,\omega,\omega)$ involves summation over different intermediate states, the resonance may result from a parity allowed, three-photon transition at $3\omega = 2.1$ eV, a parity forbidden, two-photon transition at $2\omega = 1.4$ eV, or both. All of these possibilities are consistent with previously published results [11].

Our chief experimental results are the spectroscopic measurements of the relative amplitude $\rho = \kappa_{xx}/\kappa_{xy}$ and the relative phase δ of $\chi^{(3)}_{xxxx}, \chi^{(3)}_{xxyy}$, shown in Figs. 2(a) and 2(b), respectively. These data were obtained from polarization-sensitive measurements of the third harmonic optical intensity along each of the two crystalline axes of the sample, $I_{x,y}(3\omega)$, while varying the polarization state of the fundamental laser field. In the experimental geometry used here, the incident field is initially polarized at 45° to the two crystalline axes, then passes through a polarization compensator before entering the sample. The natural axes of the compensator are aligned with those of the crystal, so the polarization state upon entering the sample is given by $\mathbf{E} = E_0[\hat{x} + \hat{y}e^{i\Delta}]/\sqrt{2}$, where Δ is the compensator retardance. Thus, the nonlinear polarizations $P_x(3\omega)$ and $P_y(3\omega)$ involve controlled mixtures of $\chi^{(3)}_{xxxx}$ and $\chi^{(3)}_{xxyy}$, with Δ as the control parameter, as may be seen through Eq. (1).

As the compensator is adjusted, the THG intensities $I_x(3\omega) \propto |P_x(3\omega)|^2$ and $I_y(3\omega) \propto |P_y(3\omega)|^2$ both oscillate sinusoidally with Δ. Results from a typical measurement, for $\hbar\omega = 0.89$ eV, are shown in the inset of Fig. 2. Straightforward manipulation of Eq. (1) tells us further that the phase offset in Δ between these two intensity curves is δ, and that the minima of $I_{x,y}(3\omega,\Delta)$ are offset from zero by $\kappa_{xy}(\rho - 3)$. From a series of such measurements at various laser frequencies, we obtain the dispersion of the relative amplitude $\rho(\omega)$ and relative phase $\delta(\omega)$, shown in Figs. 2(a) and 2(b), respectively. These data show that $\rho(\omega)$ and $\delta(\omega)$ both undergo clear, steplike changes at about 1 eV. Since these are relative quantities, we can derive the model-independent conclusion that, as the photon energy crosses $\hbar\omega \approx 1$ eV, the transition dipole elements involved in $\chi^{(3)}_{xxxx}$ and $\chi^{(3)}_{xxyy}$ connect states with different symmetry. We show below that this can only be the result of an intermediate state with a_{1g} symmetry at 2 eV.

The tensor elements of the nonlinear susceptibility are given by

$$\chi^{(3)}_{ijkl}(-3\omega;\omega,\omega,\omega) = \frac{N}{\hbar^3}\mathcal{P}_I \sum_{n=1}^{8} \times \mathcal{K}^{(n)}_{ijkl}(-3\omega;\omega,\omega,\omega), \quad (2)$$

where the intrinsic permutation operator $\mathcal{P}_I$ applies to the last three tensor indices $\{jkl\}$ [17]. The eight terms $\mathcal{K}^{(n)}$ correspond to different summations over intermediate states. The dominant term in our experiment is $\mathcal{K}^{(1)}$, which may be written

$$\mathcal{K}^{(1)}_{ijkl} = \sum_{\nu_1,\nu_2,\nu_3} \frac{\mu^i_{g\nu_1}\mu^j_{\nu_1\nu_2}\mu^k_{\nu_2\nu_3}\mu^l_{\nu_3 g}}{(\Omega_{\nu_1 g} - 3\omega)(\Omega_{\nu_2 g} - 2\omega)(\Omega_{\nu_3 g} - \omega)}, \quad (3)$$

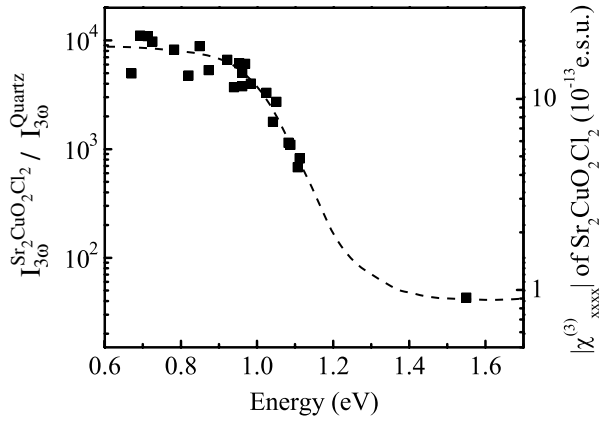

FIG. 1. Third harmonic generation in $Sr_2CuO_2Cl_2$. The left axis shows the relative values of $I(3\omega) \propto |\chi^{(3)}_{xxxx}|^2$. The right scale indicates absolute values for $Sr_2CuO_2Cl_2$. Dashed line: guide to the eye.

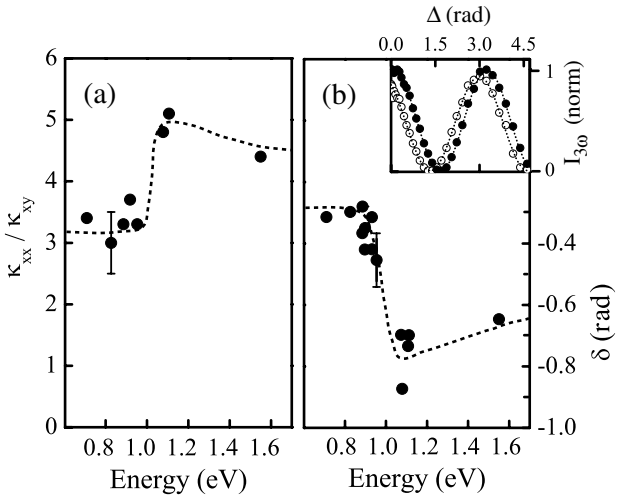

FIG. 2. (a) Relative phase δ and (b) relative magnitude ρ of $\chi^{(3)}_{xxxx}$ and $\chi^{(3)}_{xxyy}$ in $Sr_2CuO_2Cl_2$. The dashed lines are guides to the eye. Inset: Example of a retardance measurement: $I_x(3\omega)$ (filled circles) and $I_y(3\omega)$ (open circles) recorded at $\omega = 0.89$ eV. The dotted lines represent best fits to a $\sin^2$ function, from which δ and ρ are extracted.

where $\{\nu_1, \nu_2, \nu_3\}$ are the intermediate states, $\mu^i_{\nu_1\nu_2} = \langle \nu_1 | \mu^i | \nu_2 \rangle$ are dipole matrix elements along the direction $\hat{r}_i$, and each $\Omega_{\nu_\ell g} = \omega_{\nu_\ell g} - i\gamma_{\nu_\ell g}$ is a complex frequency associated with a transition from the ground state g to an intermediate state ν_j. Individual terms in Eq. (3) may be one-, two-, or three-photon resonant, or the susceptibility may contain double or triple resonances, depending on the enegy and symmetry of the states ν_ℓ. If the product of matrix elements in Eq. (3) is to be nonzero, symmetry requires both that ν_1 and ν_3 transform as e_u in $4/mmm$, and that ν_2 transforms as a_{1g} (z^2), a_{2g} $(x^3y - xy^3)$, b_{1g} $(x^2 - y^2)$, or b_{2g} (xy). Moreover, the summation over all possible permutations in Eq. (2) leads to additional cancellations, so that those terms in which ν_2 transforms as a_{2g} or b_{2g} do not contribute to the THG signal. Consequently, the even-parity intermediate states which contribute to the THG signal are exclusively those with a_{1g} or b_{1g} symmetry.

To evaluate the role of these intermediate states in the measured third-harmonic spectrum, we compare our results from $Sr_2CuO_2Cl_2$ to the results of a phenomenological, independent-level model, commonly used in nonlinear optics [17]. We assume that the excited states are independent levels, each with its own energy, dephasing rate, and symmetry. To obtain a realistic estimate of the matrix elements, excited state energies, and decay rates of the odd-parity states, observed in conventional linear optics, we performed a fit of four Lorentzian functions to the experimentally determined absorption spectrum [18,19]. By attributing each of these Lorentzians to a different state η_n, where n ranges from one to four, we obtain from the fit the energies E_n, dephasing rates γ_n, and dipole matrix elements μ^x_{gn} connecting each state η_n to the ground state. These parameters are listed in Table I. We emphasize that the parameters used here are chosen merely to yield a good description of the *linear* susceptibility, and subsequently remain fixed for the nonlinear susceptibility calculation using Eq. (2).

The results of this model calculation are shown as solid lines in Fig. 3. Panel 3(a) shows that the absolute magnitude of $\chi^{(3)}_{xxxx}$ exhibits a peak near 0.7 eV, roughly one third of the energy of the first odd-parity excited state η_1 of the model, as expected from a three-photon resonance. Panels 3(b) and 3(c) show that the relative amplitude and phase are completely flat as a function of frequency, with the value of the amplitude ratio ρ fixed at three, while the phase difference δ is fixed at zero. This is the behavior expected of a spherically symmetric nonlinear hyperpolarizability [20]. It should be noted that, in this case, the relative quantities ρ and δ are entirely insensitive to the details of the model parameters, because their values are determined by symmetry. We find that, in general, if the ground state possesses b_{1g} symmetry, then *any* set of excited states containing only b_{1g} and e_u symmetries will display this overall, spherically symmetric hyperpolarizability, over the entire frequency spectrum. The model, however, does give the right order of magnitude for $|\chi^{(3)}_{xxxx}|$. In the case of $Sr_2CuO_2Cl_2$, then, the magnitude of the nonlinear susceptibility is dominated by a three-photon resonance to CT excited states, and is only weakly enhanced by two-photon resonances to even-parity states [8].

While the overall magnitude and shape of the resonance in $\chi^{(3)}_{xxxx}$ is explained well with only the optically allowed CT excited states, the structure that we observe in δ and κ_{xx}/κ_{xy} implies the involvement of excitations with different symmetries. As we have seen, the only other states that may contribute to the THG signal are those with a_{1g} symmetry. Moreover, when these states are included in Eq. (2), the transitions to the a_{1g} and b_{1g} intermediate states will interfere. Since $\langle x|x|a_{1g}\rangle = \langle y|y|a_{1g}\rangle$, and $\langle x|x|b_{1g}\rangle = -\langle y|y|b_{1g}\rangle$, this interference will exhibit different behavior in $\chi^{(3)}_{xxxx}$ and $\chi^{(3)}_{xxyy}$, to produce exactly the deviations from spherical symmetry that we observe. Thus, we extend our model calculation by adding a state with a_{1g} symmetry at 2.0 eV. The additional matrix elements μ^x_{en} coupling this excited state to the four odd-parity excited

TABLE I. Energies E_n, dephasing rates γ_n, and matrix elements μ^x_{gn}, μ^x_{en} used in the model calculations described in the text.

η_n	E_n (eV)	γ_n (eV)	μ^x_{gn} (10^{-18} esu)	μ^x_{en} (10^{-18} esu)
η_1	1.96	0.25	1.86	3.72
η_2	2.44	1.75	4.00	0.80
η_3	4.00	5.75	4.70	0.94
η_4	5.00	5.75	4.11	0.82

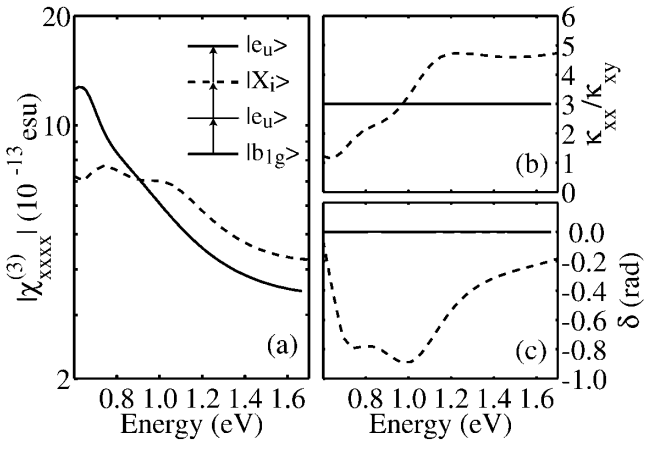

FIG. 3. Comparison of two model calculations for $\chi^{(3)}$: (a) magnitude, (b) relative amplitude ρ, and (c) relative phase δ. The inset shows the level scheme assumed in the model, with $|X_i\rangle$ the two-photon states of interest. The state $|e_u\rangle$ is a virtual excitation to the CT excitation. In all panels, solid lines indicate that only the virtual excitation to $|X_1\rangle = |b_{1g}\rangle$ is included. Dashed lines indicate the addition of a resonant state at 2.0 eV, $|X_2\rangle = |a_{1g}\rangle$.

states are given in Table I. The results shown as dashed lines in Figs. 3(b) and 3(c) are in close agreement with the experiment, both in sign and in magnitude.

The a_{1g} symmetry of this state, determined unambiguously by our analysis, is consistent with two distinct, correlation-induced excitations, an s-wave CT exciton [7] and a Cu $d_{x^2-y^2} \rightarrow d_{3z^2-r^2}$ exciton [13]. As the copper oxide plane is doped, we would expect the energy of the CT exciton to fall rapidly compared to the energy of the dd exciton, and the technique that we have described here can be used to track these changes as the Mott metal-insulator transition is approached. Coupled modes, such as an exciton-phonon (i.e., $a_{1g} \in e_u \otimes e_u$), may also be involved, via resonance phenomena, though in THG the resonant character would be strikingly different from that of Raman spectroscopy [21]. As our theoretical understanding of these excitations grows, our estimate of the matrix elements μ_{en}^{x} may help to further discriminate among symmetry-allowed possibilities, as well as shed light on the mechanism for producing large nonlinear optical susceptibilities in one-dimensional Mott insulators [8].

In $Sr_2CuO_2Cl_2$, however, it is likely that *all* of these excitations are present near 2 eV, and are strongly mixed. This proposal is supported by the independent observation of a broad Urbach tail at low temperatures, which indicates strong phonon coupling between the CT exciton and another, optically forbidden, excitation nearby in energy [19]. This could also explain earlier difficulties in observing these states, as the mixing would broaden them. Anomalously broad Urbach tails appear in many other correlated insulators, suggesting that optically forbidden states such as the one observed here may play a generic role in the linear optical properties of these systems. Future studies of related materials, in which the relative positions of the CT and dd excitons vary, will help to disentangle the relative contributions of each to the THG signal and to the Urbach tail. Such material surveys of the symmetry and energy of correlation gap states can also focus theoretical research on the magnetic, electronic, and phonon interactions that influence them. Nonlinear optical techniques can play a pivotal role in such studies, given their sensitivity to both even- and odd-parity excitations [8,10].

We summarize with a discussion of THG and conventional Raman spectroscopy, both of which are related to the third order nonlinear optical susceptibility. Unlike spontaneous Raman scattering, THG is a coherent process that returns the system to the ground state. This coherence results in a signal that is emitted into a small solid angle, making it easier to detect than the scattered light in a conventional Raman experiment. In contrast to previous Raman work, our measurements were performed with fundamental frequencies well away from resonance, and the polarization-sensitive measurements have enabled the estimation of optical matrix elements that couple the even-parity state to the optical CT gap. Ultimately, both Raman and THG spectroscopy are simply different one-dimensional cuts through the full, three-dimensional frequency space that $\chi^{(3)}$ may probe. In the future, the techniques described here may be extended to the fully general case, in which all three input photon energies and polarizations are separately controlled, thereby exploiting most fully the information contained in the $\chi^{(3)}$ tensor.

This work was supported by the U.S. Department of Energy under Contracts No. DE-AC03-76SF00098 and No. W-7405-Eng-82. Support from the German National Merit Foundation (A. B. S.), and the Deutsche Forschungsgemeinschaft (R. A. K.) are gratefully acknowledged, as is the assistance of Z. Rek, Z. Hussain, and X. Zhou for orienting the $Sr_2CuO_2Cl_2$ platelet. We thank G. A. Sawatzky and M. V. Klein for their comments on the manuscript.

*Also: Institut für Angewandte Physik, Universität Karlsruhe, 76128 Karlsruhe, Germany.

†Present address: Department of Physics, Simon Fraser University, Burnaby, BC V5A 16S, Canada.

[1] P. W. Anderson, Science **235**, 1196 (1987).
[2] M. Z. Hasan *et al.,* Science **288**, 1811 (2000).
[3] C. M. Varma, Phys. Rev. B **55**, 14 554 (1997).
[4] M. Grilli *et al.,* Phys. Rev. Lett. **67**, 259 (1991).
[5] M. E. Simón *et al.,* Phys. Rev. B **54**, R3780 (1996).
[6] F. C. Zhang and K. K. Ng, Phys. Rev. B **58**, 13 520 (1998).
[7] E. Hanamura, N. T. Dan, and Y. Tanabe, Phys. Rev. B **62**, 7033 (2000).
[8] H. Kishida *et al.,* Nature (London) **405**, 929 (2000).
[9] G. P. Zhang, Phys. Rev. Lett. **86**, 2086 (2001).
[10] A. Schülzgen *et al.,* Phys. Rev. Lett. **86**, 3164 (2001).
[11] M. A. Kastner *et al.,* Rev. Mod. Phys. **70**, 897 (1998).
[12] R. Liu *et al.,* Phys. Rev. Lett. **71**, 3709 (1993).
[13] P. Kuiper *et al.,* Phys. Rev. Lett. **80**, 5204 (1998).
[14] D. S. Chemla and J. Zyss, *Nonlinear Optical Properties of Organic Molecules and Crystals* (Academic, New York, 1987).
[15] L. L. Miller *et al.,* Phys. Rev. B **41**, 1921 (1990).
[16] J. P. Hermann, Opt. Commun. **9**, 74 (1973).
[17] R. W. Boyd, *Nonlinear Optics* (Academic, San Diego, 1992), 9th ed.
[18] H. S. Choi *et al.,* Phys. Rev. B **60**, 4646 (1999).
[19] R. Lövenich *et al.,* Phys. Rev. B **63**, 235 104 (2001).
[20] P. D. Maker and R. W. Terhune, Phys. Rev. **137**, A803 (1965).
[21] D. Salamon *et al.,* Phys. Rev. B **51**, 6617 (1995).